

# Analysis of optimal reconstruction methods based on incomplete information from sensor nodes using Kalman filter

Yanqiu Huang, *Member, IEEE*, Wanli Yu, *Student Member, IEEE*, Muhammad Usman, *Student Member, IEEE*, Shengdi Wang, and Alberto Garcia-Ortiz, *Member, IEEE*

**Abstract**—In order to reduce the communication cost of wireless sensor nodes, many methods have been proposed to reduce the transmission rate and reconstruct the signal based on incomplete information. Among them, Kalman filter (KF) based methods provide the optimal reconstruction for the monitoring of linear systems with Gaussian noise. They require sensor nodes to intermittently transmit either the raw data or the preprocessed data mainly depending on nodes' processing capabilities. However, it is unclear whether the improvement of the reconstruction quality after using local processing is significant enough to compensate the energy overhead. To solve this question, this work studies three KF-based reconstruction solutions under different transmission strategies, considering the measurement noise, the transmission rate reduction and the packet loss. The reconstruction quality of each method is formulated with the help of Markov chain and a set of algebraic Riccati equations (AREs); the corresponding energy cost of the sensor node is further measured by the physical implementation. The results indicate that the advantage of using local processing is very sensitive to some parameters, e.g., the packet size. In addition, the three KF-based methods are compared with compressive sensing. Both simulation and experimental results demonstrate the superiority of the KF-based approaches for the analyzed linear systems.

**Index Terms**—Wireless sensor nodes, Kalman filter, energy conservation, linear systems, compressive sensing.

## I. INTRODUCTION

THE combination of sensing and wireless communication technologies has enabled a wide range of applications [1]. Due to the limited resources of wireless sensor nodes, energy efficiency is typically the primary concern for almost any application [2]–[4]. As widely recognized, one of the most energy-intensive processes for a sensor node is radio communication [1]. Besides the energy consumption of data packets transmission, extra energy is also required by overhead activities, such as control packets, idle listening, overhearing, collision, etc., as analyzed in [5]. Thus, reducing the transmission rate is an efficient strategy to decrease the communication cost. However, the reduction of the transmission rate leads to the loss of information for the users. How to reconstruct

the signal based on incomplete information is an important research topic.

The typical solutions for transmission rate reduction and reconstruction are either model-based [6]–[12] or sampling/transforming-based [13]–[15]. Time series forecasting and stochastic modeling are two common model-based approaches. Based on the established model, the sink is able to predict the future data without periodically receiving the data packet from a sensor node. To guarantee the prediction accuracy, the same model is usually implemented by the sensor node simultaneously and when an event happens, e.g., the error is larger than a threshold, an update is transmitted to the sink. However, these model-based methods either are sensitive to the reliability of the wireless communication for model updating [6]–[9] or require intensive computation overhead to construct the probability models [10]–[12]. Alternatively, the transmission rate can be reduced with the help of sampling or transform theories [13]–[15]. The traditional methods usually require the sensor node to store enough samples and transmit fewer data after preprocessing [13], [14], which causes extra delay in the network. In contrast, a novel sensing theory, named compressive sensing (CS) [15], achieves sample-with-compress. When the signal is sparse in a basis expansion, the sampling rate of the sensor node can be significantly below the Nyquist rate and the sink node can reconstruct the original signal with the incomplete information. Nevertheless, the quality of the reconstructed signals may be unable to satisfy the accuracy requirements in addition to the complexity of the reconstruction algorithm.

Besides the respective drawback of each above mentioned method, one common limitation of them is that they can only supply approximations of the raw measurements, which are inevitably corrupted by noise in practical applications [1], [16]. It makes the reconstructions obtained using these schemes unable to reflect the true state of the monitored system. In this sense, the approaches based on the filtering techniques could produce more accurate reconstructions by removing the noise. When the monitored system satisfies a state space model with normal distributed noise, the Kalman filter (KF) provides the optimal state estimate from the noisy measurements in the sense of minimum mean square error (MMSE) [17].

A number of approaches have been proposed to reduce the transmission rate based on KF [18]–[20], [22]–[25]. The sensor node can either transmit the raw data [18], [26] or the preprocessed data by using a local KF [19], [20], [22]–

Y. Huang, W. Yu, and A. Garcia-Ortiz are with the Institute of Electrodynamics and Microelectronics, University of Bremen, Bremen, Germany (e-mail: huang@item.uni-bremen.de; wyu@item.uni-bremen.de; agarcia@item.uni-bremen.de).

M.Usman is with Infineon Technologies AG, 85579 Neubiberg, Germany. Shengdi Wang is with the Institute of Telecommunication and High-Frequency Techniques, University of Bremen, Bremen, Germany (e-mail: wang@ant.uni-bremen.de).

[25] and the signal is optimally reconstructed in the sink node. For instance, in [18] each sensor node intermittently transmits the raw data with a Bernoulli distribution and the signal is optimally reconstructed with a modified KF. A stochastic event-triggered transmission schedule is proposed in [26]. Each node transmits the raw data following a stochastic decision based on a uniformly distributed random variable over  $[0, 1]$ . This schedule holds the Gaussian property and the optimal reconstruction solution is obtained using a variation of the standard KF. A dual KF (DKF) approach is presented in [19]. Each node firstly uses a local KF to remove the measurement noise and to produce the optimal system output estimate. Then a pair of KFs are executed synchronously in the receiver and sender to predict the output estimate and guarantee the prediction accuracy, respectively. When the prediction error is beyond the threshold, the output estimate is transmitted to the receiver. This method is further improved by PKF [20]. The dual KFs are replaced by a pair of  $k$ -step ahead KF predictors and the local state estimate is transmitted instead of the output estimate. PKF reduces the computation cost of DKF [19] but also improves its reconstruction quality as analyzed in [22] and [23]. Considering a packet loss channel, a transmission schedule is obtained in [24] by solving an optimization problem. It decides whether each sensor node should transmit the local estimate from the KF or not. In [25], the sensor node can randomly send either the raw data or the local state estimate using a KF depending on the computation capability of the sensor.

Although those KF-based approaches can reduce the transmission rate and optimally reconstruct the signal with the incomplete information, there is a lack of comprehensive comparison between different transmission strategies. The common decision whether to transmit the raw data or the preprocessed information is solely dependent on the computation capability of the sensor node [25], [26]. However, we believe that the achieved performance should be also considered. The performance of the rate reduction scheme is usually measured by the trade-off between the reconstruction quality and the transmission rate [19], [20]. While under the same transmission rate, the energy consumption of each method could be different. Intuitively, intermittently transmitting the preprocessed information, such as state estimates of a local KF, may provide better reconstruction quality under the same transmission rate. However, considering the computation cost of a local KF and the potential transmission cost increment due to the increased packet size, it is unclear whether the improvement of the reconstruction quality is significant enough to compensate the energy overhead in practice. This work aims to analyze and compare the optimal reconstruction methods under different transmission contents (with and without preprocessing) in terms of the trade-off between reconstruction quality and energy cost. Instead of finding the best compression strategy, the comparison is restricted to the simplest random sampling scheme as in CS [15] and the packet loss model as in [18]. The main contributions include:

- a) This work studies three different transmission options and provides the corresponding optimal reconstruction solu-

tions, considering the noise, the transmission compression and the packet loss for the sensor nodes monitoring linear dynamic systems. In contrast to the approaches that only provide the approximations of noisy measurements, these methods reconstruct the signal optimally in terms of MMSE using KF.

- b) The reconstruction quality of each method is analyzed and compared under the same transmission rate reduction scheme and packet loss model. Precise formulas for the relation between reconstruction quality and system parameters, transmission rate and packet loss probability are provided.
- c) The physical implementation in the motes is conducted and the energy consumption of each method is measured. Thereby, the performances of three KF-based methods are compared in terms of the trade-off between energy cost and reconstruction quality.

The rest of this paper is organized as follows. Section II formulates the problem. Section III presents three MMSE estimate solutions under different transmission strategies and analyzes the reconstruction quality of each method. In Section IV, the analyses are firstly validated and the reconstruction quality of the three methods are compared. Then the physical implementation is conducted to measure the energy consumption and compare their performance in terms of the trade-off between reconstruction quality and energy cost. Finally, we conclude the work in Section V.

## II. PROBLEM SETUP

This section aims to formulate precisely the problem described in the introduction. The transmission rate reduction scheme and the packet loss model are firstly formulated. After studying the transmission contents, three reconstruction problems are then presented.

Considering a linear dynamic system, the system state at time  $k$ , denoted as  $x_k$ , evolves from the state at time  $k - 1$ , namely:

$$x_k = A_k x_{k-1} + w_k \quad (1)$$

where  $A_k$  is the transition matrix;  $w_k \sim N(0, Q_k)$  accounts for the inexactitudes of the model and has covariance  $Q_k$  (see e.g. [17]). The observation of the sensor node at time  $k$ , denoted as  $z_k$ , is mapped from  $x_k$  by the observation matrix  $H_k$  and corrupted with a zero mean white Gaussian noise  $v_k$ :

$$z_k = H_k x_k + v_k \quad (2)$$

where  $v_k \sim N(0, R_k)$  has the covariance  $R_k$ . These two kinds of noise are mutual uncorrelated and also uncorrelated with the state:

$$E[w_k v_j^T] = 0 \quad E[x_k w_j^T] = 0 \quad E[x_k v_j^T] = 0, \quad \forall j, k \quad (3)$$

The system is assumed to be observable. We aim to optimally reconstruct the real system output  $H_k x_k$  in the server, taking the noise and the following two factors into account: first, it is inefficient for the sensor node to transmit every data packet due to the expensive communication cost; second, the transmitted packets may be lost caused by the unreliable channel. Following CS [15], in this paper we restrict ourselves to

the simplest compression strategy where each node randomly selects some time points to transmit. Let the random variable  $\tau_k$  denote whether the sample is transmitted at time  $k$  or not:  $\tau_k = 1$  if a packet is transmitted, otherwise  $\tau_k = 0$ . It satisfies a Bernoulli distribution with probability  $p$  for the value 1, i.e.  $p_{\tau_k}(1) = p$ . The decision at time  $k$  does not affect the decision at time  $j$  ( $\forall j \neq k$ ), i.e.,  $\tau_k$  is independent of  $\tau_j$ . Regarding the model for packet loss, we adopt the scheme presented in [18], where each packet can get lost independently and is successfully received with the probability  $\lambda$ . Let the random variable  $\gamma_k$  represents whether the packet is successfully received or not. It has probability distribution  $p_{\gamma_k}(1) = \lambda$  and is independent of  $\gamma_j$  ( $\forall j \neq k$ ). Then, the binary variable  $\tau_k \gamma_k$  denotes whether the packet is received in the server and the sequence of the binary variables from time 1 to time  $k$ ,  $\Upsilon_{\mathbf{k}} = [\tau_1 \gamma_1, \tau_2 \gamma_2, \dots, \tau_k \gamma_k]$ , represents the packet reception process.

When the sensor node continuously transmits the raw data to the server, the best estimate of the system output is  $\hat{z}_k = E[z_k | \mathbf{Z}_{\mathbf{k}}]$ , where  $\mathbf{Z}_{\mathbf{k}} = [z_1, z_2, \dots, z_k]$  is the collection of the raw data till time  $k$ , since the conditional expectation is the best predictor in the sense of minimizing the mean square error [27]. With the help of the joint normal distribution, we can firstly obtain the optimal state estimation  $\hat{x}_k = E[x_k | \mathbf{Z}_{\mathbf{k}}]$  following the standard KF equations [17]:

$$\hat{x}_k^- = A_k \hat{x}_{k-1} \quad (4)$$

$$P_k^- = A_k P_{k-1} A_k^T + Q_k \quad (5)$$

$$K_k = P_k^- H_k^T (H_k P_k^- H_k^T + R_k)^{-1} \quad (6)$$

$$\hat{x}_k = \hat{x}_k^- + K_k (z_k - H_k \hat{x}_k^-) \quad (7)$$

$$P_k = (I - K_k H_k) P_k^- \quad (8)$$

Then, the optimal output estimate is  $\hat{z}_k = H_k \hat{x}_k$ . However, when the compression strategy and the packet loss are considered, transmitting the raw data may be neither the only nor the best option to precisely reconstruct the system output. To offset the effect of the missing data on the reconstruction quality, the node can preprocess the raw data with a local KF firstly and transmit more accurate data at the expense of the computation cost. In general, there are many transmission options after using KF. Here, we consider two extreme cases, transmitting either  $\hat{z}_k$  or  $\hat{x}_k$ . The former has the same size as the raw data and is the closest to the real system output and the latter has different size but is the optimal representation of the system state. Then, the sensor node can transmit one of the following three contents:  $z_k$ ,  $\hat{z}_k$  and  $\hat{x}_k$ . Assuming the node transmits the raw data, each sample  $z_k$  has the probability  $p$  to be transmitted and the packet will arrive at the server through the channel with the probability  $\lambda$  according to our compression strategy and channel loss model, as shown in Fig. 1a. Then the received data at time  $k$  in the server, denoted as  $y_k$ , is either  $z_k$  or nothing. Thus, the received data sequence till time  $k$  in the server,  $\mathbf{Y}_{\mathbf{k}} = [y_1, y_2, \dots, y_k]$ , is a subset of  $\mathbf{Z}_{\mathbf{k}} = [z_1, z_2, \dots, z_k]$ . Similarly, when the node transmits  $\hat{z}_k$  or  $\hat{x}_k$ ,  $\mathbf{Y}_{\mathbf{k}}$  is a subset of  $\hat{\mathbf{Z}}_{\mathbf{k}} = [\hat{z}_1, \hat{z}_2, \dots, \hat{z}_k]$  or  $\hat{\mathbf{X}}_{\mathbf{k}} = [\hat{x}_1, \hat{x}_2, \dots, \hat{x}_k]$ ; the corresponding diagrams are depicted in Figs. 1b and 1c, respectively.

Our goal is to firstly obtain the solutions for the three MMSE estimate problems assuming the above mentioned linear dynamic system Eqs. (1) and (2) and the success packet reception process  $\Upsilon_{\mathbf{k}}$ :

$$\begin{aligned} & \arg \min_{\bar{z}_k} E \left[ \|\bar{z}_k(\mathbf{Y}_{\mathbf{k}}) - H_k x_k\|_2^2 \right] \\ & \text{subject to } \mathbf{Y}_{\mathbf{k}} \subset \begin{cases} \mathbf{Z}_{\mathbf{k}}, & \text{if } z_k \text{ is transmitted} \\ \hat{\mathbf{Z}}_{\mathbf{k}}, & \text{if } \hat{z}_k \text{ is transmitted} \\ \hat{\mathbf{X}}_{\mathbf{k}}, & \text{if } \hat{x}_k \text{ is transmitted} \end{cases} \end{aligned}$$

where  $\bar{z}_k(\mathbf{Y}_{\mathbf{k}})$  is the estimator of  $H_k x_k$ , which is a function of the received data  $\mathbf{Y}_{\mathbf{k}}$ .

Using the properties of conditional expectation [27],  $E[H_k x_k | \mathbf{Y}_{\mathbf{k}}]$  is closest to  $H_k x_k$  of all functions of  $\mathbf{Y}_{\mathbf{k}}$  in the sense of MMSE. Thus, the problem is actually to find  $\bar{z}_k = H_k E[x_k | \mathbf{Y}_{\mathbf{k}}]$  for each transmission option. After that, we further compare the performance of the obtained solutions through the analysis of reconstruction quality and energy cost in the following sections.

### III. MMSE RECONSTRUCTION SOLUTIONS AND ANALYSIS OF RECONSTRUCTION QUALITY

This section presents the MMSE reconstruction solutions in the server, KF-raw, KF-output and KF-state, when the node randomly transmits the raw data, the estimate of the system output and the state estimate over the above mentioned packet loss channel. After that, it further formulates the reconstruction quality of each method as a function of system parameters, as well as transmission and reception probabilities.

#### A. Minimum State Estimate Covariance Filter

In [18] the authors have derived the minimum state estimate covariance filter given the observations and their arrival sequence, i.e.  $\bar{x}_k = E[x_k | \mathbf{Z}_{\mathbf{k}}, \gamma_{\mathbf{k}}]$ , where  $\gamma_{\mathbf{k}} = [\gamma_1, \dots, \gamma_k]$  satisfies a Bernoulli process. The fundamental theorem behind the core idea is that the conditional distribution of the bivariate normal is still normal [21]. More specifically, if  $[\mathbf{x}_1, \mathbf{x}_2]^T$  satisfies a joint normal distribution with mean  $[\boldsymbol{\mu}_1, \boldsymbol{\mu}_2]^T$  and covariance  $\begin{bmatrix} \boldsymbol{\Sigma}_{11} & \boldsymbol{\Sigma}_{12} \\ \boldsymbol{\Sigma}_{21} & \boldsymbol{\Sigma}_{22} \end{bmatrix}$ , then the distribution of  $\mathbf{x}_1$  conditional on  $\mathbf{x}_2 = \mathbf{a}$  is still normal and satisfies  $(\mathbf{x}_1 | \mathbf{x}_2 = \mathbf{a}) \sim \mathcal{N}(\bar{\boldsymbol{\mu}}, \bar{\boldsymbol{\Sigma}})$ , where the conditional mean and covariance can be calculated by:

$$\bar{\boldsymbol{\mu}} = \boldsymbol{\mu}_1 + \boldsymbol{\Sigma}_{11} \boldsymbol{\Sigma}_{22}^{-1} (\mathbf{a} - \boldsymbol{\mu}_2) \quad (9)$$

$$\bar{\boldsymbol{\Sigma}} = \boldsymbol{\Sigma}_{11} + \boldsymbol{\Sigma}_{12} \boldsymbol{\Sigma}_{22}^{-1} \boldsymbol{\Sigma}_{21} \quad (10)$$

Similar to the standard KF, the random variable  $z_k$  and  $x_k$  conditional on the received data  $\mathbf{Z}_{\mathbf{k}-1}$  and on the arrivals  $\gamma_{\mathbf{k}-1}$  have jointly normal distribution. The only difference is that the covariance of  $z_k$  ( $\mathbf{Z}_{\mathbf{k}-1}, \gamma_{\mathbf{k}-1}$ ) changes from  $H_k P_k^- H_k^T + R_k$  to  $s_k$ , where

$$s_k = H_k P_k^- H_k^T + \gamma_k R_k + (I - \gamma_k) \sigma^2 I \quad (11)$$

and  $\sigma^2$  is the covariance of the measurement noise when there is no update. Using Eqs. (9) and (10) and taking the limit  $\sigma^2 \rightarrow \infty$ , we can obtain the minimum state estimate covariance filter,

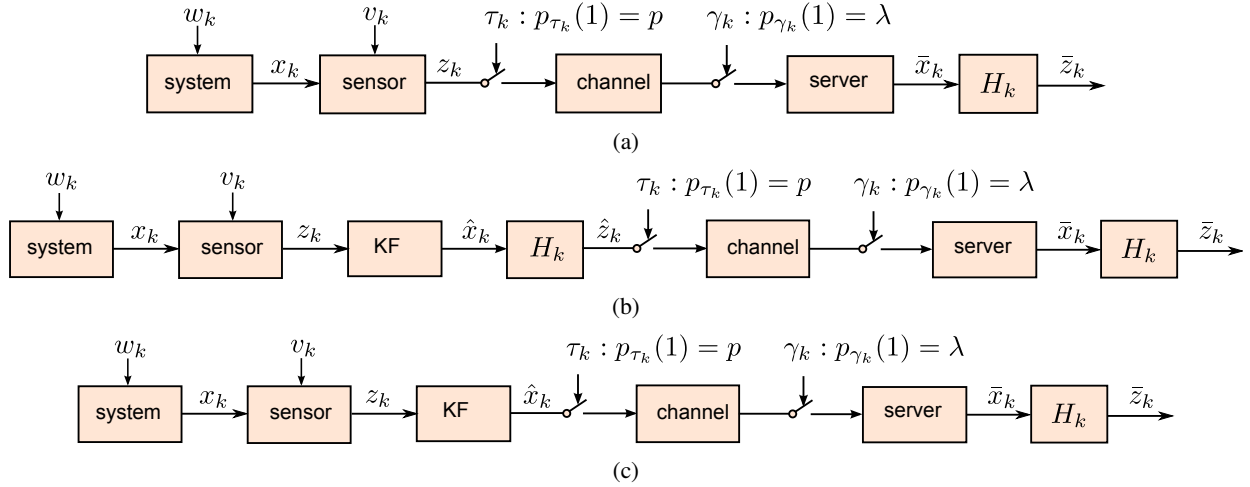


Fig. 1: Three reconstruction problems in the server, when the sensor node randomly transmits (a) the raw data; (b) the local estimate of the system output; (c) the local state estimate, with the transmission probability  $p$  over a packet drop channel, where the success arriving probability of the packet is  $\lambda$ .

Eqs. (12) to (16), but removing  $\tau_k$  in Eqs. (15) and (16). Compared with the standard KF Eqs. (4) to (8), the new filter only performs the time update (*a priori* estimation) if the measurement is not received. It minimizes the state estimate covariance given the measurements  $\mathbf{Z}_k$  and the arrivals  $\gamma_k$ .

### B. MMSE Reconstruction Solutions

We firstly provide the optimal reconstruction, named KF-raw, when  $\mathbf{Y}_k \subset \mathbf{Z}_k$ . The method from [18] can be used. Compared with [18], the only difference is that we have an additional variable  $\tau_k$  to reduce the transmission rate. However, since  $\tau_k$  has a Bernoulli distribution, it only changes Eq. (11) to  $s_k = H_k P_k^- H_k^T + \tau_k \gamma_k R_k + (I - \tau_k \gamma_k) \sigma^2 I$ . Thus, the modified KF that minimizes the state estimate covariance given a realization of  $\mathbf{Y}_k$  is:

$$\bar{x}_k^- = A_k \bar{x}_{k-1} \quad (12)$$

$$\bar{P}_k^- = A_k \bar{P}_{k-1}^- A_k^T + Q_k \quad (13)$$

$$\bar{K}_k = \bar{P}_k^- H_k^T (H_k \bar{P}_k^- H_k^T + R_k)^{-1} \quad (14)$$

$$\bar{x}_k = \bar{x}_k^- + \tau_k \gamma_k \bar{K}_k (y_k - H_k \bar{x}_k^-) \quad (15)$$

$$\bar{P}_k = \bar{P}_k^- - \tau_k \gamma_k \bar{K}_k H_k \bar{P}_k^- \quad (16)$$

The corresponding MMSE estimation of the system output is  $\bar{z}_k = E[z_k | \mathbf{Y}_k = Y_0] = H_k \bar{x}_k$  where  $Y_0$  is a realization of received data sequence.

Next, we aim to find the MMSE estimation, KF-output, when  $\mathbf{Y}_k \subset \hat{\mathbf{Z}}_k$ . Combining Eqs. (1), (2), (4) and (7), the local state estimate at time  $k$  can be described as:

$$\begin{aligned} \hat{x}_k &= K_k H_k A_k x_{k-1} + (I - K_k H_k) A_k \hat{x}_{k-1} \\ &+ K_k H_k w_k + K_k v_k \end{aligned} \quad (17)$$

It has colored noise w.r.t. the real system state:

$$\begin{aligned} \varepsilon_k &= (I - K_k H_k) A_k \varepsilon_{k-1} \\ &+ (K_k H_k - I) w_k + K_k v_k \end{aligned} \quad (18)$$

In order to obtain the optimal reconstruction when the reception is  $\hat{z}_k = H_k \hat{x}_k$ , the original system state needs to be firstly augmented [28] to include the local state estimation  $\hat{x}_k$ , namely  $X_k = [x_k, \hat{x}_k]^T$ . Then the expanded system model and the new observation model become:

$$X_k = F_k X_{k-1} + W_k \quad (19)$$

$$\hat{z}_k = C_k X_k \quad (20)$$

where  $F_k = \begin{bmatrix} A_k & \mathbb{0} \\ K_k H_k A_k & (I - K_k H_k) A_k \end{bmatrix}$ ,  $W_k = \begin{bmatrix} w_k \\ K_k H_k w_k + K_k v_k \end{bmatrix}$ ,  $C_k = [\mathbb{0} \ H_k]$ , with the covariance of the system noise  $\bar{Q}_k = \begin{bmatrix} Q_k & Q_k H_k^T K_k^T \\ K_k H_k Q_k & K_k R_k K_k^T \end{bmatrix}$  and the covariance of the observation noise  $\bar{R}_k = 0$ . The optimal reconstruction of the system state can thereby be obtained using Eqs. (12) to (16) by changing the system parameters. Note that, this produces actually the estimation of the expanded state,  $\bar{X}_k$ , whose first element is the final estimation of the real system state. Then the MMSE estimate of the system output using KF-output is:

$$\bar{z}_k = E[z_k | \hat{\mathbf{Z}}_k, \mathbf{Y}_k = \Upsilon_0] = [H_k \ \mathbb{0}] \bar{X}_k \quad (21)$$

When the node randomly transmits the local state estimation over the packet dropping channel, namely  $\mathbf{Y}_k \subset \hat{\mathbf{X}}_k$ , the MMSE estimate of the system state at time  $k$  is:

$$\bar{x}_k = E[x_k | \mathbf{Y}_k \subset \hat{\mathbf{X}}_k] = \begin{cases} \hat{x}_k, & \text{if } \tau_k \gamma_k = 1 \\ A_k \bar{x}_{k-1}, & \text{otherwise} \end{cases} \quad (22)$$

This means that the server only needs to perform a linear predictor:

$$\bar{x}_k = A_k \bar{x}_{k-1} \quad (23)$$

and replaces the prediction  $\bar{x}_k$  by  $\hat{x}_k$ , if the packet is received. The reconstructed system output is then  $\bar{z}_k = E[z_k | \mathbf{Y}_k \subset \hat{\mathbf{X}}_k] = H_k \bar{x}_k$ . This method is called KF-state.

In summary, when the node randomly transmits the raw data (with the transmission probability  $p$  of each sample) over the packet loss channel (with the successful reception probability  $\lambda$ ) as depicted in Fig. 1a, the MMSE estimation of the system state  $\bar{x}_k$ , can be obtained using KF-raw with Eqs. (12) to (16); when the local estimated system output is transmitted as shown in Fig. 1b, KF-output uses the modified KF with the expanded system parameters in Eqs. (19) and (20) produces the optimal estimation of the augmented state, whose first element corresponds to the MMSE estimation of the original system state,  $\bar{x}_k$ ; when the local estimated state is transmitted as indicated in Fig. 1c, the MMSE estimation  $\bar{x}_k$  is produced by KF-state using the linear predictor Eq. (23) with the replacement when the data packet is received. The corresponding MMSE estimation of the system output using these three methods can be obtained by  $\bar{z}_k = H_k \bar{x}_k$ .

### C. Analyses of Reconstruction Quality

The reconstruction error,  $\epsilon_k = H_k x_k - \bar{z}_k$ , at each time  $k$  is a random variable and we use its covariance,  $\bar{\sigma}$ , to measure the reconstruction quality of each method. It depends on the system parameters,  $A_k$ ,  $H_k$ ,  $R_k$ ,  $Q_k$ , as well as the transmission and reception probabilities  $p$  and  $\lambda$ . This section aims to formulate their relations considering a time invariant system. The analysis consists of three steps. Firstly, we partition the errors coming from different time instant  $k$  into different groups with the help of Markov chain and the calculation of  $\bar{\sigma}$  is converted to obtain the error covariance and probability at each Markov state using the law of total probability. Secondly, the problem is further simplified to calculate the error covariance of the state estimate at state 0 using the relation between the covariance at state  $i$ , and state at  $i - 1$ . For KF-state, the solution is straightforward, while for KF-raw and KF-output, the third step is required. An explicit equation between the covariance at state 0 and the covariance at other states is formulated and an approximation is further provided.

We firstly group the errors into different Markov states and formulate  $\bar{\sigma}$  following the ideas presented in [22], [23]. Note that even the fundamental theory is similar, here we solve a different problem. The reconstruction of the server at each time instant  $k$ ,  $\bar{z}_k$ , is a random variable. It could be either the *a priori* prediction or the *a posteriori* estimate depending on  $\tau_k \gamma_k$ . Let  $\beta_k$  be the binary random variable for each  $k$ : if the outcome is the *a priori* prediction,  $\beta_k = 1$  corresponds to a *success*; otherwise,  $\beta_k = 0$  corresponds to a *failure*. Then the probability of a failure is  $p\lambda$  at each time instant  $k$ , since each packet has  $p\lambda$  probability to be received. The value of  $\beta_k$  does not affect the likelihood of getting  $\beta_{k+1} = 1$  or  $\beta_{k+1} = 0$  at time  $k + 1$ . In other words, each binary random variable is identical and independent. It is associated with a Bernoulli trial and the sequence of the independent binary random variables  $\{\beta_1, \beta_2, \beta_3, \dots\}$  is a Bernoulli process. Let  $\theta_k$  denote the number of most recent consecutive successes that have been observed at the  $k$ th trial. If the  $k$ th trial is a failure, then  $\theta_k = 0$ ; if trial numbers  $k, k-1, \dots, k-m+1$  are all successes but trial number  $k-m$  is a failure, then  $\theta_k = m$ . For example,

considering we obtain  $\{\beta_1, \beta_2, \beta_3, \beta_4, \dots\} = \{0, 1, 1, 0, \dots\}$  in an experiment, then  $\theta_1 = \theta_4 = 0$ ,  $\theta_2 = 1$  and  $\theta_3 = 2$ . The collection of  $\{\theta_1, \theta_2, \theta_3, \dots\}$  is thereby a stochastic process. Assuming  $\theta_k = i$  at the  $k$ th trial, then  $\theta_{k+1}$  will equal either  $i+1$  or 0 at the next trial regardless of the values  $\theta_1, \dots, \theta_{k-1}$ . It means the random process satisfies the Markov property and can be modeled as a discrete-time Markov chain as shown in Fig. 2. The state space of the Markov chain is  $\mathbb{N}$ , which is the set of all possible values of  $\theta_k$ .

According to the law of total probability,  $\bar{\sigma} = \text{cov}(\epsilon_k)$ , is the summation of the product of the probability that  $\epsilon_k$  locates at each state,  $p_i = p(\epsilon_k | \theta_k = i)$ , and the covariance of the errors at each state,  $\sigma_i = \text{cov}(\epsilon_k | \theta_k = i)$ , namely:

$$\begin{aligned} \bar{\sigma} &= \text{cov}(\epsilon_k) = \sum_{i=0}^{\infty} p(\epsilon_k | \theta_k = i) \text{cov}(\epsilon_k | \theta_k = i) \\ &= \sum_{i=0}^{\infty} p_i \sigma_i = \sum_{i=0}^{\infty} p_i H \Sigma_i H^T \end{aligned} \quad (24)$$

where  $\Sigma_i = \text{cov}(x_k - \bar{x}_k)$  is the error covariance of the state estimate produced at state  $i$  and  $\sigma_i = H \Sigma_i H^T$ . The goal of obtaining  $\bar{\sigma}$  gets reduced to calculate  $p_i$  and  $\Sigma_i$ . Note that,  $\bar{\sigma}$  and  $\Sigma_i$  can also be represented by  $\bar{P}_k$  in the modified KF in Eq. (16). Since  $\bar{P}_k = E[(x_k - \hat{x}_k)(x_k - \hat{x}_k)^T | \Upsilon_k = \Upsilon_0]$  is a function of the received data sequence, it is a random variable. Then  $\bar{\sigma} = \text{cov}(\epsilon_k) = E[(H x_k - \bar{z}_k)(H x_k - \bar{z}_k)^T | \Upsilon_k] = H E[\bar{P}_k] H^T$  and  $\Sigma_i = E[\bar{P}_k | \theta_k = i]$ .

For calculating  $p_i$ , the transition matrix of the Markov chain is needed. The transition probability of going from state  $i$  at time  $k$  to the next state  $i + 1$  at time  $k + 1$  is  $\Pr(\theta_{k+1} = i + 1 | \theta_k = i) = 1 - p\lambda$ . It is actually independent of the time instant, namely, the transition probability from state  $i$  at any time instant  $j$  to state  $i + 1$  is  $1 - p\lambda$ . Thus, we can discard the time instant to obtain the transition probability from state  $i$  to state  $i + 1$ :

$$\begin{aligned} p_{i,i+1} &= \Pr(\theta_{k+1} = i + 1 | \theta_k = i) \\ &= \Pr(\theta_{j+1} = i + 1 | \theta_j = i) \\ &= 1 - p\lambda \end{aligned} \quad (25)$$

The transition probability from state  $i$  to state 0 has the probability  $p_{i,0} = p\lambda$  as shown in Figure 2. Thus, the transition

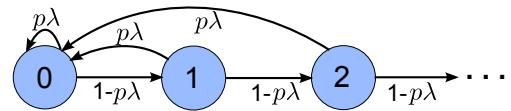


Fig. 2: State graph of the success-runs chain when the sensor node randomly transmits data over the packet drop channel.

matrix of the chain is:

$$P = \begin{pmatrix} p\lambda & 1-p\lambda & \dots & 0 & 0 & \dots \\ \vdots & \vdots & \ddots & \vdots & \vdots & \ddots \\ p\lambda & 0 & \dots & 1-p\lambda & 0 & \dots \\ \vdots & \vdots & \ddots & \vdots & \vdots & \ddots \end{pmatrix}$$

It is a time-homogeneous Markov chain. The distribution over the states can be written as a stochastic row vector  $\boldsymbol{\pi} = [p_0, p_1, p_2 \dots]$  with non-negative entries that add up to one. The probability of the random variable  $\theta_k$  at the state  $i$  is  $\Pr(\theta_k = i) = \boldsymbol{\pi}(i) = p_i$ . According to the steady state equation,  $\boldsymbol{\pi}P = \boldsymbol{\pi}$ , we can obtain the distribution over the state  $i$ :

$$p_i = p_{i-1}(1 - p\lambda) = p\lambda(1 - p\lambda)^i \quad (26)$$

The probability at state 0,  $p_0 = p\lambda$ , is the reception rate of the receiver.

Now we calculate  $\Sigma_i$ . Assuming  $\theta_{k-1} = i - 1$  and  $\theta_k = i$ ,  $i \in \mathbb{N}^+$ , the error covariance of the state estimate at time  $k$  is evolved from the error covariance at time  $k - 1$  satisfying Eq. (13). Thus,  $\Sigma_i$  can be calculated from  $\Sigma_{i-1}$  using:

$$\Sigma_i = A\Sigma_{i-1}A^T + Q = g_i(\Sigma_0) \quad (27)$$

where  $g_i(\Sigma_0) = A^i\Sigma_0A^{iT} + \sum_{j=0}^{i-1} A^jQA^{jT}$ . Thus, to obtain the final reconstruction error covariance  $\bar{\sigma}$ , only the error covariance of the state estimate produced at state 0,  $\Sigma_0$ , is needed.

For **KF-state**,  $\Sigma_0$  is straightforward. It equals the converged covariance matrix of the local KF, i.e.,  $\Sigma_0 = \lim_{k \rightarrow \infty} P_k = P$ . Since once the update  $\hat{x}_k$  is received, the prediction at time  $k$  is replaced and the estimate covariance  $\bar{P}_k$  is calibrated to  $P$ , no matter which state is the prediction from. More specifically,

$$\bar{P}_k = \begin{cases} P, & \text{if } \tau_k \gamma_k = 1 \\ A\bar{P}_{k-1}A^T + Q, & \text{otherwise} \end{cases} \quad (28)$$

Thus, we can easily calculate the exact  $\bar{\sigma}$  using (26) and (27) for **KF-state**. While, for **KF-raw** and **KF-output**, the state estimation error can not be calibrated when there is an update. In the following, we aim to find the equation between  $\Sigma_0$  and  $\Sigma_i$  ( $i = 1, 2, \dots$ ) at other states. Once the equation is solved, the only unknown  $\Sigma_0$  can be obtained.

We start at **KF-raw** and the same method is suitable for **KF-output** as presented later. The error at state 0 may come from any state  $i$  ( $i \in \mathbb{N}$ ), whenever there is an update (i.e., a successful reception) as shown in Fig. 2. Let  $\Sigma_{i0}$  denote the covariance of the errors coming from state  $i$  to state 0. It is derived from the *a priori* prediction covariance  $\Sigma_{i0}^-$  at state  $i$  following Eq. (13), with an update phase following Eqs. (14) and (16):

$$\Sigma_{i0}^- = A\Sigma_iA^T + Q = g_{i+1}(\Sigma_0) \quad (29)$$

$$K = \Sigma_{i0}^- H^T (H\Sigma_{i0}^- H^T + R)^{-1} \quad (30)$$

$$\Sigma_{i0} = (I - KH)\Sigma_{i0}^- \quad (31)$$

Then the covariance at state 0,  $\Sigma_0$ , is the summation of the product of the probability at each state and the covariance of the errors coming from each state to state 0, namely

$$\Sigma_0 = \sum_{i=0}^{\infty} p_i \Sigma_{i0} \quad (32)$$

Combining Eqs. (27) to (31), we obtain:

$$\Sigma_0 = \sum_{i=0}^{\infty} p_i \left[ g_{i+1}(\Sigma_0) - g_{i+1}(\Sigma_0)H^T (Hg_{i+1}(\Sigma_0)H^T + R)^{-1} Hg_{i+1}(\Sigma_0) \right] \quad (33)$$

Although there is only one unknown  $\Sigma_0$  in this equation, it is nontrivial to solve it. We validate this equation empirically in the next section and propose an approximate solution here. The idea is to separate the summation in Eq. (33) into a set of independent equations and solve each equation to obtain the approximate result of  $\Sigma_{i0}^-$ , thereby calculating the approximate  $\Sigma_{i0}$ ,  $\Sigma_0$  and  $\bar{\sigma}$  using the former presented equations. The following assumption is made for the approximation: as long as the error at state 0 comes from state  $i$ ,  $\Sigma_{i0}$  is fixed and equals the converged covariance when the node transmits every  $i + 1$  samples. In other words, the assumption overlooks the effects of the errors from other states ( $\forall j \neq i$ ) on the changes of  $\Sigma_0$ . It is equivalent to split the state graph with infinite states in Fig. 2 into a set of cyclic graphs as shown in Fig. 3. More specifically, it corresponds to multiply a  $p_i$  in the left side of Eq. (33) for each state  $i$  and the summation is separated into a set of independent equations:

$$p_i \Sigma_0 = p_i \left[ g_{i+1}(\Sigma_0) - g_{i+1}(\Sigma_0)H^T (Hg_{i+1}(\Sigma_0)H^T + R)^{-1} Hg_{i+1}(\Sigma_0) \right] \quad (34)$$

where  $i = 0, 1, 2, \dots$ . Each of them is an algebraic Riccati equation (ARE), after replacing the unknown  $\Sigma_0$  by  $\Sigma_{i0}^- = g_{i+1}(\Sigma_0)$  with the help of Eqs. (27) and (29), namely:

$$\Sigma_{i0}^- = A^{i+1}\Sigma_{i0}^-A^{i+1T} - A^{i+1}\Sigma_{i0}^-H^T (H\Sigma_{i0}^-H^T + R)^{-1} H\Sigma_{i0}^-A^{i+1T} + \sum_{j=0}^i A^jQA^{jT} \quad (35)$$

It provides an approximation of the real  $\Sigma_{i0}^-$  and can be solved using the generalized eigenproblem algorithms [29]. Plugging this result into Eqs. (30) and (31), we can obtain the approximate  $\Sigma_{i0}$ . Then the approximate  $\Sigma_0$  can be further calculated using Eq. (32). Combining with Eqs. (26), (27) and (24), the approximate estimate covariance  $\bar{\sigma}$  can be derived.

The analysis of the reconstruction quality using **KF-output** follows the same procedure as **KF-raw**. The difference is that we have to firstly obtain the estimate covariance of the augmented state,  $\bar{\Sigma}$ , by substituting all the expanded system parameters into Eqs. (24) to (35). Then  $\bar{\sigma}$  can be further calculated by:

$$\bar{\sigma} = [H \quad 0] \bar{\Sigma} [H \quad 0]^T \quad (36)$$

In summary, the reconstruction quality of the system state is represented by the estimate covariance  $\bar{\sigma}$ . For **KF-raw**, it can be derived using Eqs. (24) to (33) for the exact solution, which is nontrivial to calculate. An approximate solution is provided by solving a set of AREs in Eq. (35) firstly and then combining with Eqs. (30) to (32) and Eqs. (26), (27) and (24). For **KF-output**, the estimate covariance of the augmented state can be obtained using the same method. We have to further

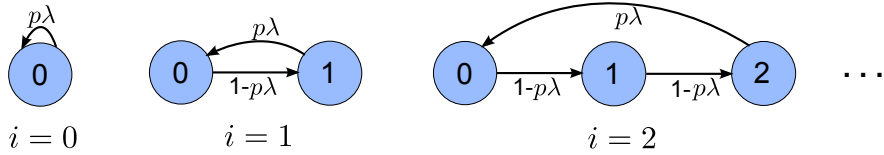


Fig. 3: A set of cyclic state graphs of the success-runs chain for calculating the approximate estimate covariance.

extract  $\bar{\sigma}$  with the help of Eq. (36). For KF-state, the exact  $\bar{\sigma}$  can be easily calculated using Eqs. (26), (27) and (24) with  $\Sigma_0 = P$ .

#### IV. SIMULATION AND EXPERIMENTAL RESULTS

This section provides the simulation and experimental results. It validates the analyses of the reconstruction quality in Section III-C and further provides the energy cost including the computation and communication measured from the physical implementation. Moreover, they are compared with CS [15] in terms of the reconstruction quality of the system output signal. In the simulation section, an artificial system is firstly created with an exact state space representation and its output is sparse in the frequency domain to avoid the validation and comparison biases caused by the uncertainty of the system model. In the experimental section, the physical implementation is conducted with the notes to collect real sensor signals for further validation and comparison in reality. Moreover, the energy cost including computation and communication are measured. The trade-off between the energy cost and the reconstruction quality is further provided under a typical scenario.

##### A. Analyses Validation and Reconstruction Comparison Using An Artificial System

This section validates the analyses in Section III-C and compares the reconstruction quality of each method using the simulated system. Besides, it provides a comparison of KF-based methods and CS under the random sampling scheme. For the sake of fairness, the created system has the state space representation and its output is sparse in the frequency domain. One example of the randomly created system in Matlab with  $2^{14}$  samples has the system parameters listed in Table I. It is generated based on the state space representation of the quadrature sinusoid signals with the frequency  $f = 200$  Hz and the sampling frequency  $F_s = 1$  kHz, but with the changed transition matrix<sup>1</sup>  $A = \begin{bmatrix} \cos(2\pi f/F_s) & \sin(2\pi f/F_s) \\ -\sin(2\pi f/F_s) & 0.9 \cos(2\pi f/F_s) \end{bmatrix}$  to make the system stable (eigenvalues of the  $A$  matrix within the unit circle). The pseudo noise  $w_k$  drawn from the standard normal distribution with the covariance  $Q$  is added to the state. Fig. 4a depicts the measured signal of the system in the time domain, which has the measurement noise  $v_k \sim \mathcal{N}(0, R)$ . It is approximately sparse in the frequency domain due to the added noise as shown in Fig. 4b using Fourier transformation. The transmission rate  $p$  is adjusted from 0.1 to 1 and the successful reception probability is set to  $\lambda = 0.9$ . Under each transmission probability, 100 experiments are conducted. We firstly validate the analysis for each method using this

<sup>1</sup>This will only change the phase of the sinusoid but not the frequency.

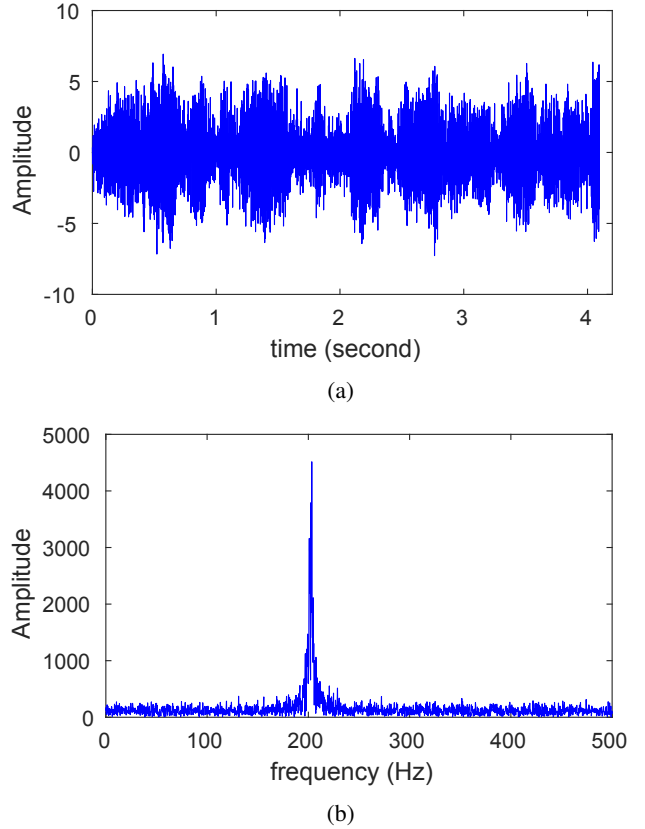


Fig. 4: (a) The noisy measurements of the generated system in time domain; (b) Single-sided amplitude spectrum of the noisy measurements in frequency domain using the Fourier transformation.

system. As mentioned in Section III-C, there exists actually two alternatives to calculate the reconstruction covariance empirically: the first one is to directly calculate the covariance of the reconstruction error compared with the real system output; the second one is through the use of  $\bar{P}_k$  matrix. We firstly compare them as shown in Figs. 5a to 5c and they perfectly match with each other when the system satisfies the given state space model. This can be treated as a metric to measure if the system model is accurate or not. Later on, we use the direct calculation as the empirically results. Regarding the exact analysis, when the node randomly transmits the raw data and the estimated output, Eq. (33) is nontrivial to calculate as mentioned in Section III-C. Here we plug the obtained  $\Sigma_0$  from all experiments to prove its correctness.

Figs. 6a to 6c depict the trade-offs between transmission rate and reconstruction quality of these three methods. The empirical results precisely match the analysis using Eqs. (26)

TABLE I: The system parameters of an artificial system with sparse represented output.

$A$	$H$	$R$	$Q$
[0.3090, 0.9511; -0.9511, 0.2781]	[0.2660, 0.3695]	0.9345	[0.5284, 9e-4; 9e-4, 0.0296]

to (33). The approximated results of  $\Sigma_0$  in KF-raw and KF-output using Eq. (34), overestimate the error at each state, which degrades the estimation of the covariance. For example, when the transmission probability is  $p = 0.5$ , we obtain 15 states (from state 0 to state 14) in Fig. 2 due to the limited length of the experiment. The distribution of the probability at each state is listed in Table II. As the sequence number of the state increases, the probability at each state decreases. It confirms the analysis calculated from Eq. (26). The reconstruction error covariance at each state  $\sigma_i$  from the experiment and the analysis, are reported in Figs. 7a to 7c, for KF-raw, KF-output and KF-state, respectively. The difference among them becomes larger, when the sequence number of the Markov state gets bigger. This is because that the empirical calculation is inaccurate, due to too few samples at the bigger number states (see Table II). For example, there is only one sample at state 14, which results in a 0 covariance at this state using the unbiased estimator of the population covariance. However, it does not drastically affect the results of the final covariance  $\bar{\sigma}$ , since the probabilities at these states are relative small. For example,  $\bar{\sigma}$  of KF-output is 0.3632 obtained empirically and 0.3649 analytically. There are discrepancies between the approximated results and the exact analyses of KF-raw and KF-output. This is caused by the approximation of  $\Sigma_{i0}^-$ . The approximated  $\Sigma_{i0}^-$  obtained from Eq. (35) actually corresponds to the converged covariance under any given initial value, rather than the covariance of the  $(i+1)$  step ahead prediction error evolved from  $\Sigma_0$ , i.e.,  $g_{i+1}(\Sigma_0)$ .

Next, we compare these three methods with CS [15]. For initiating CS [15], the discrete Fourier transform (DFT) matrix is exploited as the representation basis,  $\Psi$ , since the output signal is actually the linear combination of  $\sin(2\pi f/F_s)$  and  $\cos(2\pi f/F_s)$  added with Gaussian noise. The sensing matrix  $\Phi \in \mathbb{R}^{p\lambda L \times L}$  selects the time points of  $\mathbf{Z}_k$  that has been successfully received. It can be constructed using an  $L \times L$  identity matrix, where each row  $k$  has  $p\lambda$  probability to be selected depending on whether the value of  $\tau_k \gamma_k = 1$ . Due to the approximate sparse representation and the measurement noise, the reconstruction problem can be formulated as a basis pursuit denoising (BPDN) problem to find the sparse representation of  $H\mathbf{X}_k$  from  $\mathbf{Y}_k$ , denoted as  $\hat{\mathbf{Z}}_k$ , with smallest  $\ell_1$ -norm, subject to the approximately known loss  $\|\phi\psi\hat{\mathbf{Z}}_k - \mathbf{Y}_k\|_2 \leq \delta$ :

$$\begin{aligned} & \arg \min_{\hat{\mathbf{Z}}_k} \|\hat{\mathbf{Z}}_k\|_1 \\ & \text{subject to } \|\phi\psi\hat{\mathbf{Z}}_k - \mathbf{Y}_k\|_2 \leq \delta \end{aligned} \quad (37)$$

where  $\delta = \sqrt{p\lambda LR}$  due to the measurement noise has zero mean and variance  $R$ . We use [31] to solve this problem. After obtaining  $\hat{\mathbf{Z}}_k$ , the reconstructed signal is  $\psi\hat{\mathbf{Z}}_k$  with the reconstruction covariance  $\text{cov}(\psi\hat{\mathbf{Z}}_k - H\mathbf{X}_k)$ .

The trade-off between the covariance of the reconstructed signal  $\bar{\sigma}$  and the transmission rate  $p$  is depicted in Fig. 8. We firstly compare the three KF-methods. Under a given trans-

mission rate, KF-output achieves better reconstruction than KF-raw. Since when the local estimated output  $\hat{z}_k$  is received, the reconstruction error of the output signal is calibrated, i.e., the reconstruction covariance produced at the Markov state 0,  $\sigma_0$ , is reset to the minimum value  $HPH^T$ . However, since the complete state information can not be obtained, the reconstruction error of the state still accumulates. When the local state estimation is received, the reconstruction error at state 0 can be reset to the minimum  $P$ . Therefore, KF-state achieves the best reconstruction with the lowest covariance  $\bar{\sigma}$  under the same transmission rate. The gain of KF-state increases as the transmission rate decreases, since the local state information plays a more important role in calibrating the cumulative error. For example, when  $p = 0.5$  and  $\lambda = 0.9$ ,  $\bar{\sigma}$  is 0.3345 produced by KF-state, which reduces the error covariance generated by KF-output and KF-raw by 8.56% and 26.48%, respectively; when  $p$  decreases to 0.1 and  $\lambda = 0.9$ , the corresponding gains become to 27.37% and 43.24%, respectively. Note that, if the sensor node continuously transmits and all of them are successfully received ( $p = 1$  and  $\lambda = 1$ ), there will be no missed information and thus no difference among these three methods in terms of the reconstruction quality. Compared with CS [15], all of them produce better reconstructed signal. For example, when the node randomly transmits the raw data over the unreliable channel with the transmission rate  $p = 0.5$  and  $\lambda = 0.9$ , the variance of the reconstruction  $\bar{\sigma}$  using KF-raw is only 0.4550; while using CS, it is 0.5036, which is 10.69% larger.

### B. Physical Implementation

This section implements the three methods in the motes using sensed temperature signal as an example. Besides the confirmation of the results obtained from the simulation, it further provides the energy cost of each method and compares them in terms of the trade-off between energy cost and reconstruction quality.

The experiment setup, similar to the one used in [23], is depicted in Fig. 9. It uses a server (PC) for data reconstruction and two OpenMotes [32] for sending and receiving. The OpenMote is based on the Ti CC2538 System on Chip (SoC) [33], which combines a 32-bit ARM Cortex-M3 with an IEEE 802.15.4 compliant RF transceiver in one chip. The sender is powered by the DC power supply with 3.0 V. The step-down DC-DC converter TPS62730 in the mote regulates the input voltage down to 2.1 V in the regulated mode. The receiver is connected to the server, where the data monitoring application is used to receive, display and store data. The nodes run ContikiOS, which is an open source, highly portable, multi-tasking operating system for memory-efficient networked embedded systems and wireless sensor networks [34]. The RIME communication stack is used, which provides a set of custom lightweight communication primitives designed for low-power wireless networks [35]. To attain low-power operation of the

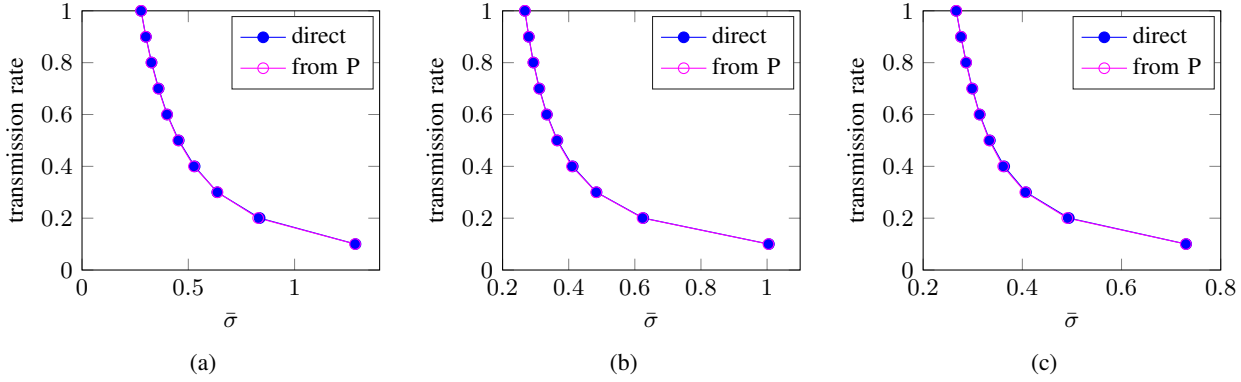


Fig. 5: System model accuracy estimation through the comparison between the directly calculated covariance of the reconstruction errors w.r.t. the real system output and the way through the use of  $\bar{P}_k$  using the artificial system for (a) KF-raw; (b) KF-output; (c) KF-state.

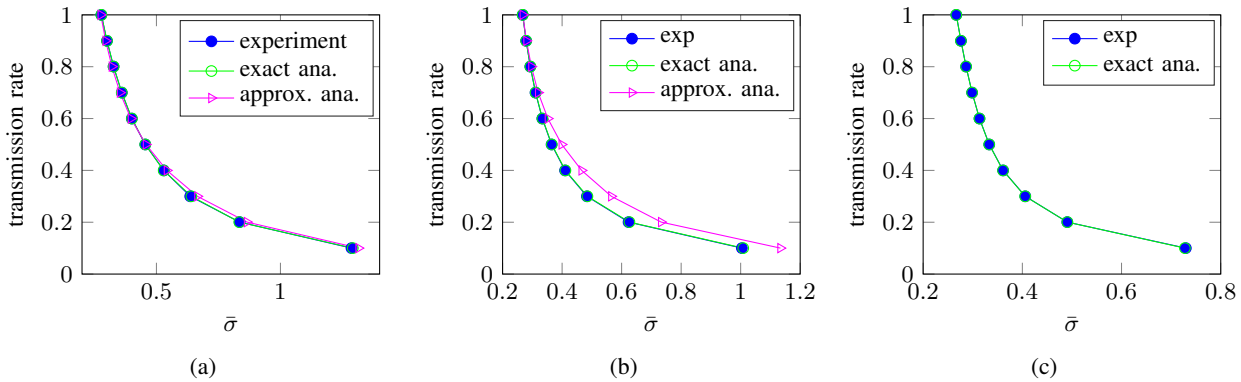


Fig. 6: The comparison of the trade-off between transmission rate and reconstruction quality obtained empirically and analytically using the artificial system, where ‘empirical’ corresponds to the direct calculation of the reconstruction error covariance; ‘exact ana.’ corresponds to Eqs. (24) to (33) and Eq. (36); ‘approx. ana.’ corresponds to Eq. (35), Eqs. (30) to (32), Eqs. (26), (27) and (24), and Eq. (36) for (a) KF-raw; (b) KF-output; (c) KF-state.

TABLE II: Comparison of the probability distribution at each Markov state using the artificial system between the empirical results and the analysis obtained from Eq. (26).

state	0	1	2	3	4	5	6	7	8	9	10	11	12	13	14
$p_i$ exp.	0.4505	0.2478	0.1347	0.0738	0.0406	0.0225	0.0133	7.4e-3	4.5e-3	2.2e-3	1.6e-3	5e-4	3e-4	2e-4	1e-4
$p_i$ ana.	0.4500	0.2475	0.1361	0.0749	0.0412	0.0226	0.0125	6.9e-3	3.8e-3	2.1e-3	1.1e-3	6e-4	3e-4	2e-4	1e-4

radio, ContikiMAC [36] is used. The node is required to keep the radio off as much as possible and periodically wake up to check for radio activity. The channel check rate (CCR) is given in Hz, specifying the number of channel checking per second. It is given in powers of two with 7 options, ranging from 2 to 128 Hz, and the default value is 8 Hz. The unicast scheme is exploited between two nodes: if a packet transmission is detected, the receiver stays awake to receive the next packet and sends an acknowledgment (ACK); to send a packet, the sender repeatedly transmits the same packet until an ACK is received.

1) *Analyses Validation and Reconstruction Comparison Using Experimental Collected Signals:* We validate the analyses and compare these three methods with CS [15] using experimental collected signal in this section. The sender collects the temperature using SHT21 sensor every minute. The server reconstructs the system state and the system output based on

the received information. The collected data in the Lab with  $L = 1638$  samples is shown in Fig. 10a. We assume the temperature changes with a velocity and use Matlab system identification toolbox [37] to find a second order state space model. The obtained system parameters are listed in Table III. For CS [15], the representation basis  $\Psi$  is different from the simulation section. The discrete cosine transform (DCT) matrix is used here, which produces better results than FFT. The signal is sparse after DCT as depicted in Fig. 10b, where 99% of the energy can be represented by the largest DCT coefficient. For confirmation of the former analyses, we manipulate the transmission rate from 0.1 to 1 and keep the successful reception probability as  $\lambda = 0.9$  using the collected signal. Under each transmission probability, 100 experiments are conducted.

We firstly analyze if the system can be accurately characterized by the obtained system model following the metric

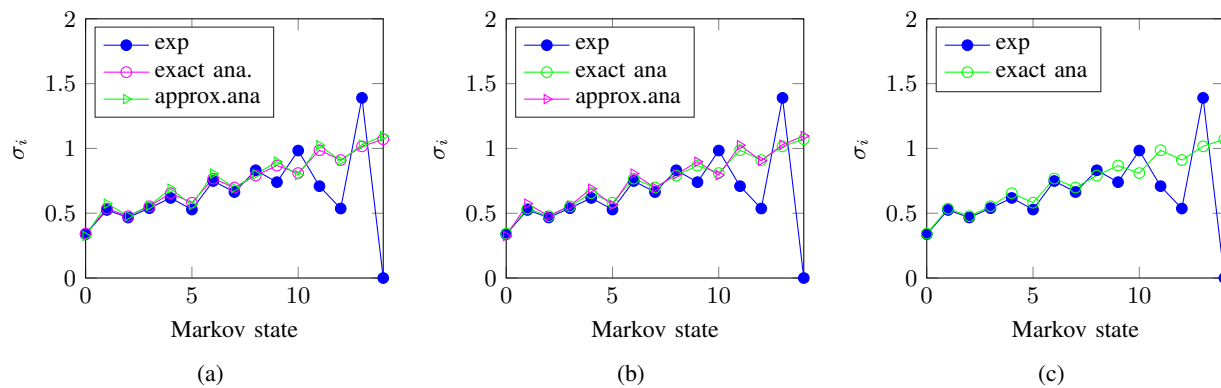


Fig. 7: The comparison of reconstruction error covariance at each Markov state,  $\sigma_i$ , obtained empirically and analytically using the artificial system, where ‘empirical’ corresponds to the direct calculation of the reconstruction error covariance; ‘exact ana.’ corresponds to Eqs. (24), (27) to (33); ‘approx. ana.’ corresponds to Eqs. (27), (30) to (32) and (35), and Eqs. (36) and (24) for (a) KF-raw; (b) KF-output; (c) KF-state.

TABLE III: The system parameters of the collected data using Openmotes.

$A$	$H$	$R$	$Q$
[0.7921, 0.8151; -0.0436, 1.1708]	[1 0]	0.4545	[0.1868, 0.0484; 0.0484, 0.0127]

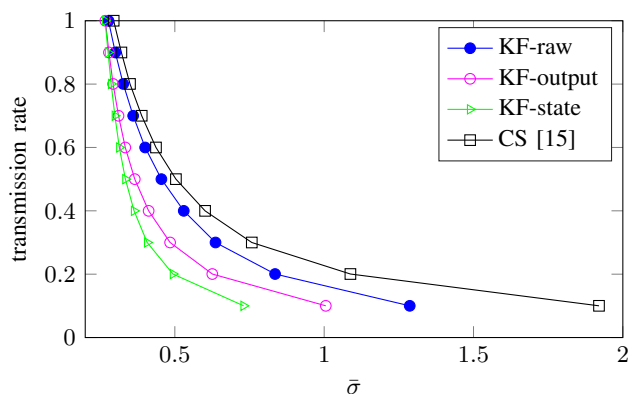


Fig. 8: The trade-off comparison between transmission rate and reconstruction quality of the system output signal among three KF methods and CS [15] using the artificial system.

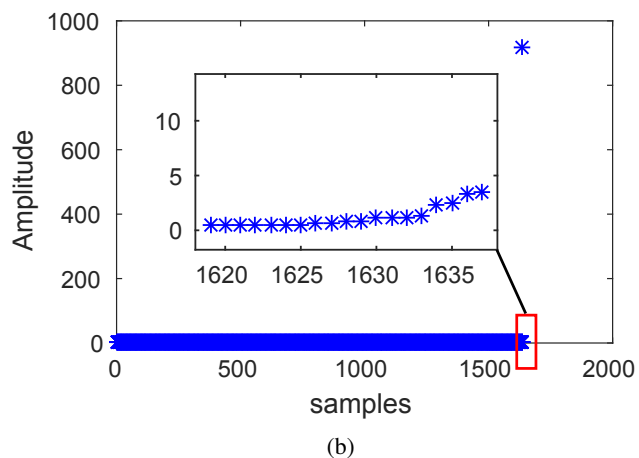
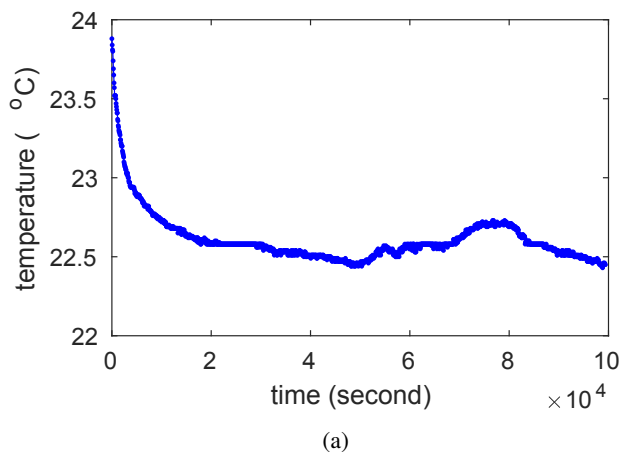


Fig. 10: (a) The collected temperature data with Openmote in the time domain; (b) The sorted amplitude spectrum of the signal using DCT in the ascending order.

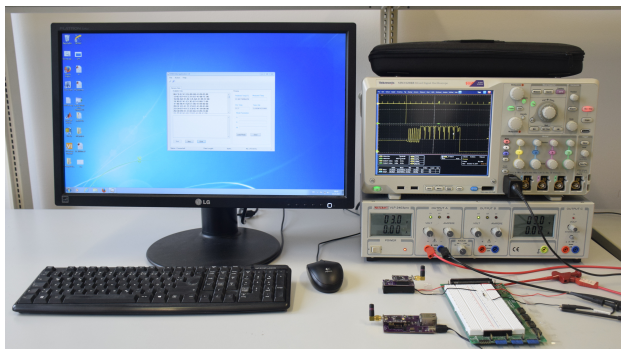


Fig. 9: Experiment setup for analyses validation and energy cost measurement using Openmotes.

described in Section IV-A. The real system output  $Hx_k$  is unknown in this situation. However, to calculate the covariance of the reconstruction error w.r.t.  $Hx_k$ , we can firstly calculate the covariance of the reconstruction error w.r.t. the KF estimated output  $\hat{z}_k$  then add the local KF estimate covariance, since  $\text{cov}(\bar{z}_k - Hx_k) = \text{cov}(\bar{z}_k - \hat{z}_k) + \text{cov}(\hat{z}_k - Hx_k) = \text{cov}(\bar{z}_k - \hat{z}_k) + HPH^T$ . Figs. 11a to 11c depict the covariance of reconstruction error w.r.t. the KF estimated output calculated using  $\text{cov}(\bar{z}_k - \hat{z}_k)$  and  $\bar{P}_k$  matrix. The two empirically obtained results are quite close for all three KF methods. Thus, the obtained model fits the data set. We add  $\text{cov}(\bar{z}_k - \hat{z}_k)$  by  $HPH^T$  to obtain the reconstruction covariance w.r.t. the real system output and to represent the empirical results later on. Similarly, the objective of CS in Eq. (37) becomes to find the sparse representation of KF estimated output, i.e.,  $\hat{Z}_k = \psi^{-1} \bar{Z}_k$ . The *a priori* information is  $\delta = \sqrt{p\lambda L(R - HPH^T)}$  according the former analysis. After obtaining  $\hat{Z}_k$  using [31], the reconstruction covariance of CS is  $\text{cov}(\psi \hat{Z}_k - \bar{Z}_k) + HPH^T$ .

The comparisons of the empirical results and the analyses for these three methods using the collected signal are presented in Figs. 12a to 12c, respectively. Although there are slightly discrepancies between the analyses and the empirical results for each method, the errors are acceptable. They are mainly due to the inaccuracy of the system model. There are no significant differences of the reconstruction quality among these three methods for this system as shown in Fig. 13: KF-raw is slightly worse than KF-output and KF-state, and the later two methods have very similar performance depending on the system parameters. While compared with CS [15], the superiority of KF-based methods are very obvious as reported in Fig. 13. The lower the transmission rate is, the higher improvements of the reconstruction quality the KF-based schemes achieve. For example, when the transmission rate equals 0.5, KF-raw reduces the reconstruction covariance of CS [15] by 56.03 %; the improvement increases to 77.9%, as the transmission rate decreases to 0.1.

2) *Comparison of Energy Cost*: This section measures the energy cost of the sensor node using these three KF methods and further compares the performance of each method in terms of the trade-off between energy cost and reconstruction quality. We firstly compare the computation cost of them. The difference among them in the sender is whether a local KF is used. In this experiment, we have implemented a 2-order KF in the sender and visualize the current profile on the Tektronix MSO5204B oscilloscope by measuring the voltage drop over a 10  $\Omega$  resistor, which is connected in series with the sender. The current profile is shown in Fig. 14. Because the execution time of a KF is very small, it is repeated 100 times in the node. It costs 26.2 *ms* in total, which corresponds to 0.262 *ms* for each execution of a KF. The voltage drop is 110.12 *mV* and corresponds to 11.012 *mA* of the current in the 10  $\Omega$  resistor. Thus the per-time current consumption by executing a KF is  $C_{comp} = 2.88 \text{mAms}$ . The corresponding energy consumption of the KF is the product of the electric charge and the regulated voltage, i.e.,  $E_{comp} = 2.1C_{comp} = 6.05 \mu\text{J}$ .

Now we measure the communication cost using these three methods. Figure 15 depicts the current profile of the sender

during a communication transaction, when the CCR of the receiver is 32 Hz. When there is a packet to be transmitted, the radio is woken up to firstly detect, if there is any data coming from other nodes to be received. Two successive clear channel assessments (CCA) are performed for this purpose with the interval  $T_c$  between them. Then a collision avoidance mechanism is conducted before data transmission, where several successive CCAs are performed to check the availability of the channel. After that, the sender starts to transmit the collected data consisting of 6 preamble and header bytes and the payload. Note that the maximum payload length is 127 bytes according to the format of IEEE 802.15.4 standard and the minimum is 43 bytes (19 bytes MAC header and 24 bytes frame payload) according to ContikiMAC. When the payload is fewer than 43 bytes, the rest will be filled with default values. Then the RF is switched from transmission to receive the ACK. Because the absence of ACK, the radio is switched to transmission again to retransmit the data packet until it receives the ACK.  $T_i$  interval is required between two consecutive transmissions. The number of retransmissions increases as the CCR of the receiver decreases, since it can not promptly detect the communication and respond the transmitter. For example, there are only 2 retransmissions in average, when the CCR of the master node is 128 Hz; the number increases to 9 and 32, when CCR decreases to 32 Hz and 8 Hz, respectively.

Since the number of total transmitted packages during one transaction is related to the CCR of the receiving node, here we firstly measure the unit transmission cost  $E_{tx\_unit}$  of the three KF methods, denoted as *Unit TX* in Fig. 15, which corresponds to the energy consumption of transmitting a single package without any retransmission. The maximum data length left for the user is  $N_{Bmax} = 108$  bytes and when the data length is smaller than 24 bytes,  $N_{Bmin} = 24$  bytes will be transmitted. Theoretically,  $E_{tx\_unit}$  can be calculated by

$$E_{tx\_unit} = e_{tx} \min(N_{Bmin}, N_B), \quad N_B \leq N_{Bmax} \quad (38)$$

where  $e_{tx}$  is the energy cost of transmitting 1 bit depending on the hardware. Fig. 16a depicts our measurement of  $E_{tx\_unit}$  for different sizes of the raw data, ranging from 1 to 54 bytes. There are slightly differences w.r.t. the theoretical results caused by the manual error. The data size when transmitting the estimated system output signal is the same as the raw data, while the size is doubled when transmitting the state estimate for a 2nd-order system. Thus, the unit transmission cost of KF-raw and KF-output are the same for any given size of the raw data. Compared with transmitting the system state, they require fewer energy when the raw data size is bigger than 12 bytes; otherwise, all of them are the same.

Taking the 32 Hz CCR of the receiver for example, we compare the trade-offs between energy cost and reconstruction quality of the three methods using the collected signal. The energy cost is measured by adding the computation cost and the communication cost per transmission. Let  $E_{cmn}$  denote the average cost per communication. It can be calculated by

$$E_{cmn} = E_o + pE_{tx\_unit}N_{tx} + E_{rx} \quad (39)$$

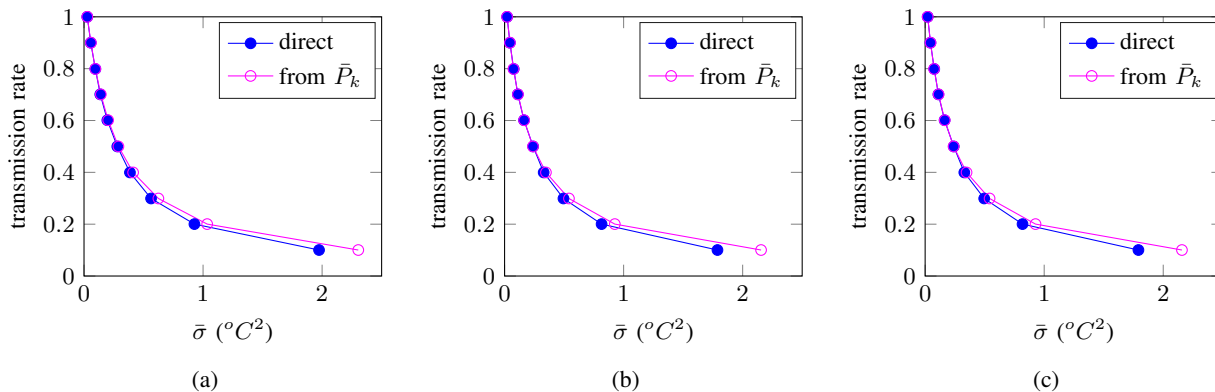


Fig. 11: System model accuracy estimation through the comparison between the directly calculated covariance of the reconstruction errors w.r.t. the KF estimate and the way through the use of  $\bar{P}_k$  using the collected signal for (a) KF-raw; (b) KF-output; (c) KF-state.

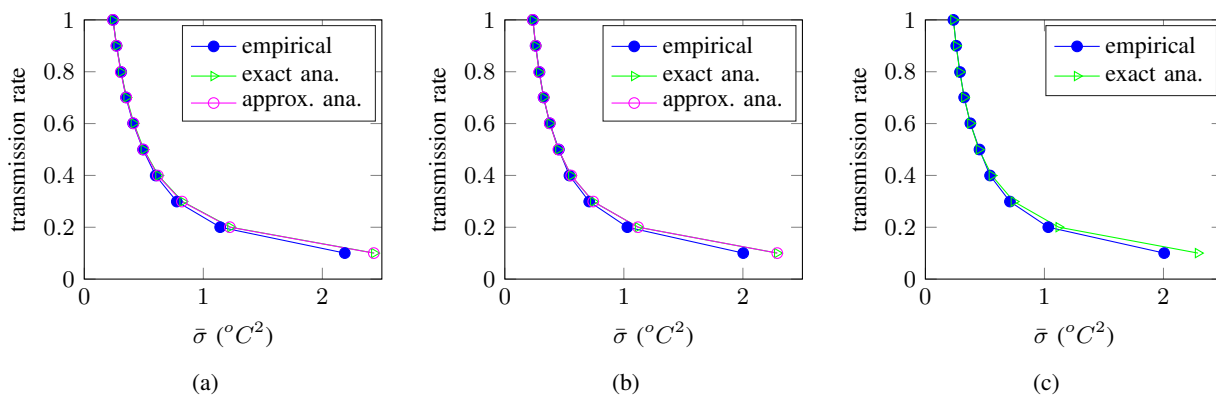


Fig. 12: The comparison of the trade-off between transmission rate and reconstruction quality obtained empirically and analytically using the collected signal, where ‘empirical’ corresponds to the direct calculation of the reconstruction error covariance; ‘exact ana.’ corresponds to Eqs. (24) to (33) and Eq. (36); ‘approx. ana.’ corresponds to Eq. (35), Eqs. (30) to (32), Eqs. (26), (27) and (24), and Eq. (36) for (a) KF-raw; (b) KF-output; (c) KF-state.

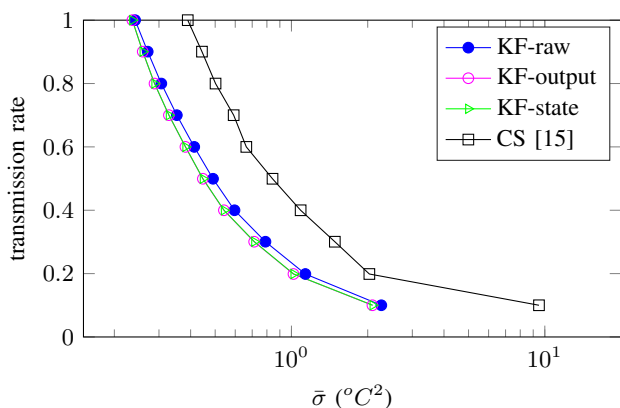


Fig. 13: Comparison of three KF methods with CS [15] in terms of reconstructing the system output signal using the experimental collected signal.

where  $E_o$  is the average overhead cost spent on CCRs before transmission, depending on the hardware and the MAC layer;  $N_{tx}$  is the average number of transmission times, mainly

depending on the MAC protocol;  $E_{rx}$  is the energy cost spent on receiving the ACK, mainly depending on the hardware. In this case,  $E_o$  is around  $224.36 \mu J$ ,  $N_{tx}$  is 9 and  $E_{rx}$  is  $14.78 \mu J$ . When the transmitted data length is fewer than 12 bytes, the trade-off between energy cost and reconstruction quality is shown in Fig. 16b. The trend is nearly the same as Fig. 13, since all of them spend the same energy on transmission and the slightly difference is caused by the additional computation cost of KF in KF-state and KF-output, which is hundredth or thousandth of the transmission cost. While as the size increases, the conclusion of the comparison among the three methods needs to be refined. For example, when the size of the raw data is 52 bytes, the trade-off between energy cost and reconstruction quality is shown in Fig. 16c. In this scenario KF-raw performs even better than KF-state in terms of the energy cost to obtain the same reconstruction quality. This example confirms our former analyses but also indicates that using the trade-off between transmission rate and reconstruction quality to compare the superiority of rate reduction techniques is not always fair. Under the same transmission rate, the energy consumption of each method could be different. In our cases, this difference is mainly caused by

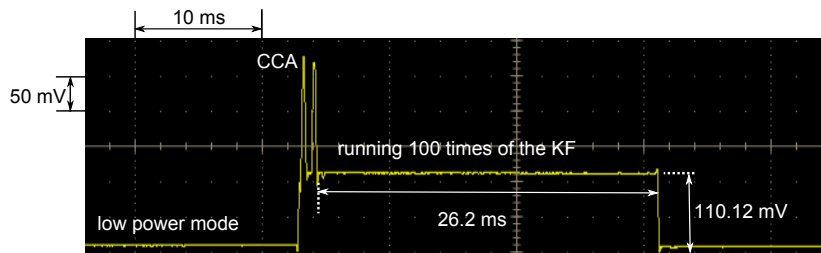


Fig. 14: The current profile of executing the 2nd-order KF 100 times visualized from the Tektronix MSO5204B oscilloscope.

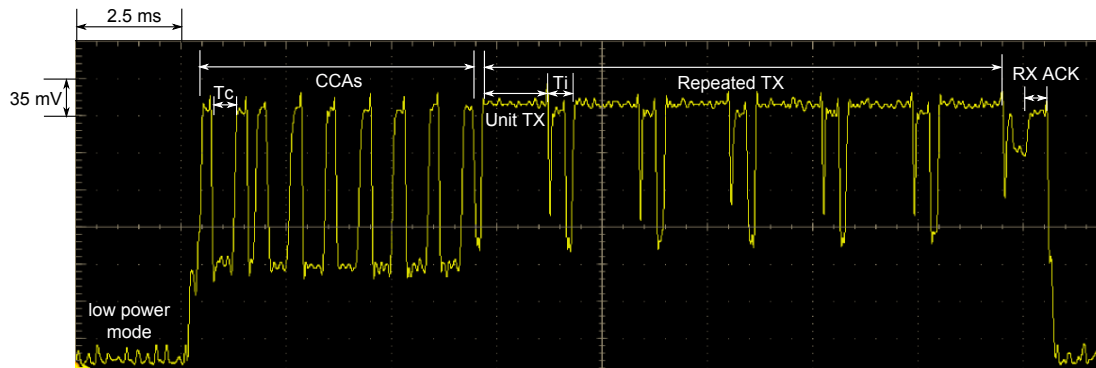


Fig. 15: The current profile of the node during a communication transaction, when the CCR of the receiver is 32 Hz.

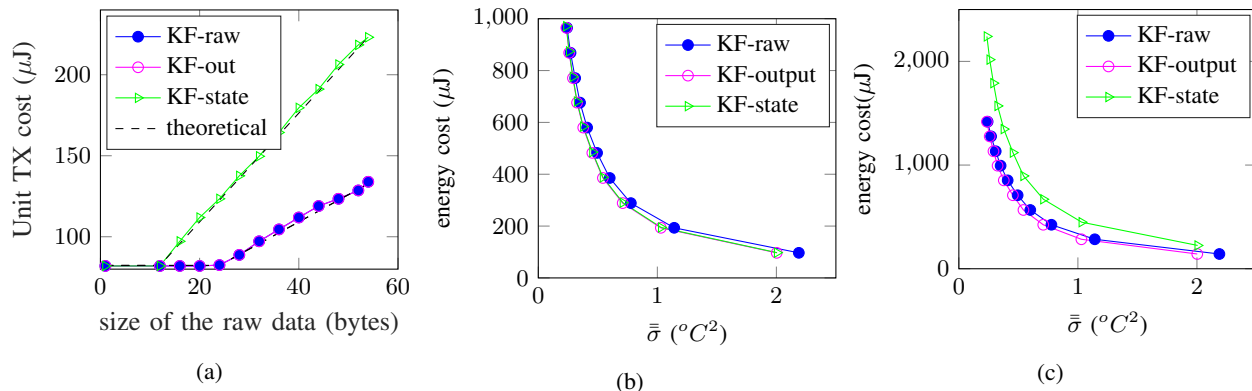


Fig. 16: (a) The unit transmission cost of three KF methods, as the size of the raw data increases from 1 to 54 bytes; (b) An example of the trade-off between the overall cost per transmission and the reconstruction quality as the transmission varies, when the CCR of the receiver is 32 Hz and the size of the raw data is smaller than 12 bytes using the experimental collected data; (c) An example of the trade-off between the overall cost per transmission, including computation and communication, and the reconstruction quality as the transmission rate varies, when the CCR of the receiver is 32 Hz and the size of the raw data is 54 bytes using the experimental collected data.

the transmission packet size.

## V. CONCLUSION AND FUTURE WORK

This paper analyzes and compares the trade-off between reconstruction quality and energy cost of different optimal reconstruction methods under different transmission options, considering the measurement noise, the transmission rate reduction and the packet loss for linear dynamic systems.

The reconstruction quality of each method is analyzed and formulated as a function of the system parameters, the transmission rate and the channel loss probability. To reduce the calculation complexity, an additional approximate solution

is provided by solving a set of AREs. The analyses are firstly validated through an artificial generated system in the simulation, where the exact state space representation of the system avoids the validation biases caused by the uncertainty of the system model. From the obtained trade-off between the transmission rate and the reconstruction quality, KF-state has the best performance. The gain increases as the transmission rate decreases. For example, when the transmission rate is  $p = 0.1$  and the packet successfully reception probability is  $\lambda = 0.9$ , KF-state decreases the reconstruction covariance of KF-output and KF-raw by 27.49% and 44.39%, respectively.

Moreover, the physical implementation is conducted in the

Openmotes. It confirms the former analyses in reality and further provides the energy cost of each method including computation and communication. The results indicate that using the trade-off between transmission rate and reconstruction quality as a metric to measure the superiority of rate reduction techniques is not always fair. Under the same transmission rate, the energy cost of each method could be different. In our experiment, the superiority of transmitting the state estimate disappears as the packet size increases due to the heavier communication energy cost. For example, when the size of the raw data is 52 bytes, KF-raw consumes even less energy than KF-state to obtain the same reconstruction quality. This also indicates that even if the sensor node has the computation capability, it is not always worthy to do local processing.

In addition, the three KF-based methods are compared with CS [15] in terms of the reconstruction quality of the system output signal. The results demonstrate their superiority for the analyzed linear systems. For example, when the transmission rate of the collected data equals 0.5, KF-based approaches reconstruct the signal by 168.6% more accurate than CS [15] and the improvement increases to 1563%, as the transmission rate decreases to 0.1.

In the future, a more detailed model to characterize the energy cost of each transmission content will be studied. Besides the current considered parameters, such as the packet size and the CCR, the system order and the communication hops also affect the energy cost. These parameters will be further integrated into the model for the performance comparison.

## REFERENCES

- [1] W. Dargie and C. Poellabauer, *Fundamentals of Wireless Sensor Networks: Theory and Practice*. John Wiley and Sons, 2010.
- [2] W. Yu and Y. Huang and A. Garcia-Ortiz, *Distributed Optimal On-Line Task Allocation Algorithm for Wireless Sensor Networks*. IEEE Sensors Journal, vol. 18, no. 1, pp.446-458, 2018.
- [3] B. Liu and Z. Zhang, *Quantized Compressive Sensing for Low-Power Data Compression and Wireless Telemonitoring*. IEEE Sensors Journal, vol. 16, no. 23, pp.8206-8213, 2016.
- [4] C. Sarkar and V. S. Rao and R. Venkatesha Prasad and S. N. Das and S. Misra and A. Vasilakos, *VSF: An Energy-Efficient Sensing Framework Using Virtual Sensors*. IEEE Sensors Journal, vol. 16, no. 12, pp.5046-5059, 2016.
- [5] Y. Huang, W. Yu, and A. Garcia-ortiz, "Accurate energy-aware workload distribution for wireless sensor networks using a detailed communication energy cost model," *Journal of Low Power Electronics*, vol. 10, no. 2, pp. 183–193(11), June 2014.
- [6] D. Tulone and S. Madden, "PAQ: Time series forecasting for approximate query answering in sensor networks," in *Proceedings of the Third European Conference on Wireless Sensor Networks*, ser. EWSN'06, Berlin, Heidelberg, pp. 21–37, 2006.
- [7] S. Santini and K. Rmer, "An Adaptive Strategy for Quality-Based Data Reduction in Wireless Sensor Networks," in *Proceedings of the Third International Conference on Networked Sensing Systems*, ser. INSS'06, Rosemont, Illinois, USA, pp. 29–36, 2006.
- [8] U. Raza, A. Camerra, A. L. Murphy, T. Palpanas, and G. P. Picco, "Practical data prediction for real-world wireless sensor networks," *IEEE Transactions on Knowledge and Data Engineering*, vol. 27, no. 8, pp. 2231–2244, Aug 2015.
- [9] Y.-A. Le Borgne, S. Santini, and G. Bontempi, "Adaptive model selection for time series prediction in wireless sensor networks," *Signal Process.*, vol. 87, no. 12, pp. 3010–3020, Dec. 2007.
- [10] A. Deshpande, C. Guestrin, S. R. Madden, J. M. Hellerstein, and W. Hong, "Model-driven data acquisition in sensor networks," in *Proceedings of the Thirtieth International Conference on Very Large Data Bases - Volume 30*, ser. VLDB '04. VLDB Endowment, pp. 588–599, 2004.
- [11] D. Chu, A. Deshpande, J. Hellerstein, and W. Hong, "Approximate data collection in sensor networks using probabilistic models," in *Data Engineering, 2006. ICDE '06. Proceedings of the 22nd International Conference on*, pp. 48–48, April 2006.
- [12] B. Kanagal and A. Deshpande, "Online filtering, smoothing and probabilistic modeling of streaming data," in *Data Engineering, 2008. ICDE 2008. IEEE 24th International Conference on*, pp. 1160–1169, April 2008.
- [13] C. Liu, K. Wu, and J. Pei, "An energy-efficient data collection framework for wireless sensor networks by exploiting spatiotemporal correlation," *Parallel and Distributed Systems, IEEE Transactions on*, vol. 18, no. 7, pp. 1010–1023, July 2007.
- [14] V. Goyal, "Theoretical foundations of transform coding," *Signal Processing Magazine, IEEE*, vol. 18, no. 5, pp. 9–21, Sep 2001.
- [15] E. Candes and M. Wakin, "An introduction to compressive sampling," *Signal Processing Magazine, IEEE*, vol. 25, no. 2, pp. 21–30, March 2008.
- [16] M. S. Obaidat and S. Misra, *Principles of Wireless Sensor Networks*. Cambridge University Press, 2014.
- [17] E. Kalman, Rudolph, "A new approach to linear filtering and prediction problems," *Transactions of the ASME—Journal of Basic Engineering*, vol. 82, no. Series D., pp. 35–45, 1960.
- [18] B. Sinopoli, L. Schenato, M. Franceschetti, K. Poolla, M. I. Jordan, and S. S. Sastry, "Kalman filtering with intermittent observations," *IEEE transactions on Automatic Control*, vol. 49, no. 9, pp. 1453–1464, 2004.
- [19] A. Jain, E. Y. Chang, and Y.-F. Wang, "Adaptive stream resource management using Kalman filters," in *Proceedings of the 2004 ACM SIGMOD International Conference on Management of Data*, ser. SIGMOD '04, New York, NY, USA, 2004, pp. 11–22.
- [20] Y. Huang, W. Yu, and A. Garcia-Ortiz, "PKF: A communication cost reduction schema based on Kalman filter and data prediction for wireless sensor networks," in *Proceedings of the 26th IEEE International system-on-chip conference*. CAS, 2013, pp. 73–78.
- [21] J. T. David Gamarnik, "Fundamentals of probability: continuous random variables," 2008. [Online]. Available: [https://ocw.mit.edu/courses/electrical-engineering-and-computer-science/6-436j-fundamentals-of-probability-fall-2008/lecture-notes/MIT6\\_436JF08 lec07.pdf](https://ocw.mit.edu/courses/electrical-engineering-and-computer-science/6-436j-fundamentals-of-probability-fall-2008/lecture-notes/MIT6_436JF08 lec07.pdf)
- [22] Y. Huang, W. Yu, C. Osewold, and A. Garcia-Ortiz, "Analysis of PKF: A communication cost reduction scheme for wireless sensor networks," *IEEE Transactions on Wireless Communications*, vol. 15, no. 2, pp. 843–856, Feb 2016.
- [23] Y. Huang, "Transmission rate compression based on Kalman filter using spatio-temporal correlation for wireless sensor networks," Ph.D. dissertation, University of Bremen, Bremen, Germany, 2017.
- [24] A. S. Leong, S. Dey, and D. E. Quevedo, "Sensor scheduling in variance based event triggered estimation with packet drops," *IEEE Transactions on Automatic Control*, vol. 62, no. 4, pp. 1880–1895, April 2017.
- [25] L. Shi, M. Epstein, and R. M. Murray, "Kalman filtering over a packet-dropping network: A probabilistic perspective," *IEEE Transactions on Automatic Control*, vol. 55, no. 3, pp. 594–604, March 2010.
- [26] D. Han, Y. Mo, J. Wu, S. Weerakkody, B. Sinopoli, and L. Shi, "Stochastic event-triggered sensor schedule for remote state estimation," *IEEE Transactions on Automatic Control*, vol. 60, no. 10, pp. 2661–2675, Oct 2015.
- [27] S. M. Kay, *Fundamentals of Statistical Signal Processing: Practical Algorithm Development*. Pearson Education, 2013, vol. 3.
- [28] A. Bryson and D. Johansen, "Linear filtering for time-varying systems using measurements containing colored noise," *IEEE Transactions on Automatic Control*, vol. 10, no. 1, pp. 4–10, Jan 1965.
- [29] W. F. Arnold and A. J. Laub, "Generalized eigenproblem algorithms and software for algebraic riccati equations," *Proceedings of the IEEE*, vol. 72, no. 12, pp. 1746–1754, 1984.
- [30] E. Candes and J. Romberg, "l1-magic: Recovery of sparse signals via convex programming," 2005.
- [31] Ewout van den Berg and Michael P. Friedlander, "Probing the Pareto Frontier for Basis Pursuit Solutions," *SIAM Journal on Scientific Computing*, vol. 31, no. 2, pp.890–912, 2009.
- [32] O. Technologies, "Openmote features," <http://www.openmote.com/hardware/openmote-cc2538-en.html>, 2015, [Online]. Accessed Dec, 30, 2017. [Online]. Available: <http://www.openmote.com/hardware/openmote-cc2538-en.html>
- [33] T. I. Incorporated, "CC2538 powerful wireless micro-controller system-on-chip for 2.4-GHz IEEE 802.15.4, 6LoWPAN, and ZigBee applications," <http://www.ti.com/lit/ds/swrs096d/swrs096d.pdf>, April 2015, [Online]. Accessed Dec, 30, 2017.

- [34] Thingsquare, “ContikiOS homepage,” <http://www.contiki-os.org/index.html>, 2015, [Online], Accessed Nov, 30, 2017. [Online]. Available: <http://www.contiki-os.org/index.html>
- [35] A. Dunkels, F. Österlind, and Z. He, “An adaptive communication architecture for wireless sensor networks,” in *Proceedings of the 5th international conference on Embedded networked sensor systems*. ACM, 2007, pp. 335–349.
- [36] M. Michel and B. Quoitin, “Technical report: Contikimac vs x-mac performance analysis,” *arXiv preprint arXiv:1404.3589*, 2014.
- [37] L. Ljung, “System identification toolbox users guide,” [https://www.mathworks.com/help/pdf\\_doc/ident/ident.pdf](https://www.mathworks.com/help/pdf_doc/ident/ident.pdf) [Online], Sep 2016, accessed Nov. 30. 2016.